Neuron, Volume *109*

Supplemental Information

Gating of hippocampal rhythms and memory by synaptic plasticity in inhibitory interneurons

Xingzhi He, Jiarui Li, Guangjun Zhou, Jing Yang, Sam McKenzie, Yanjun Li, Wenwen Li, Jun Yu, Yang Wang, Jing Qu, Zhiying Wu, Hailan Hu, Shumin Duan, and Huan Ma

Supplemental Figures

Figure S1.

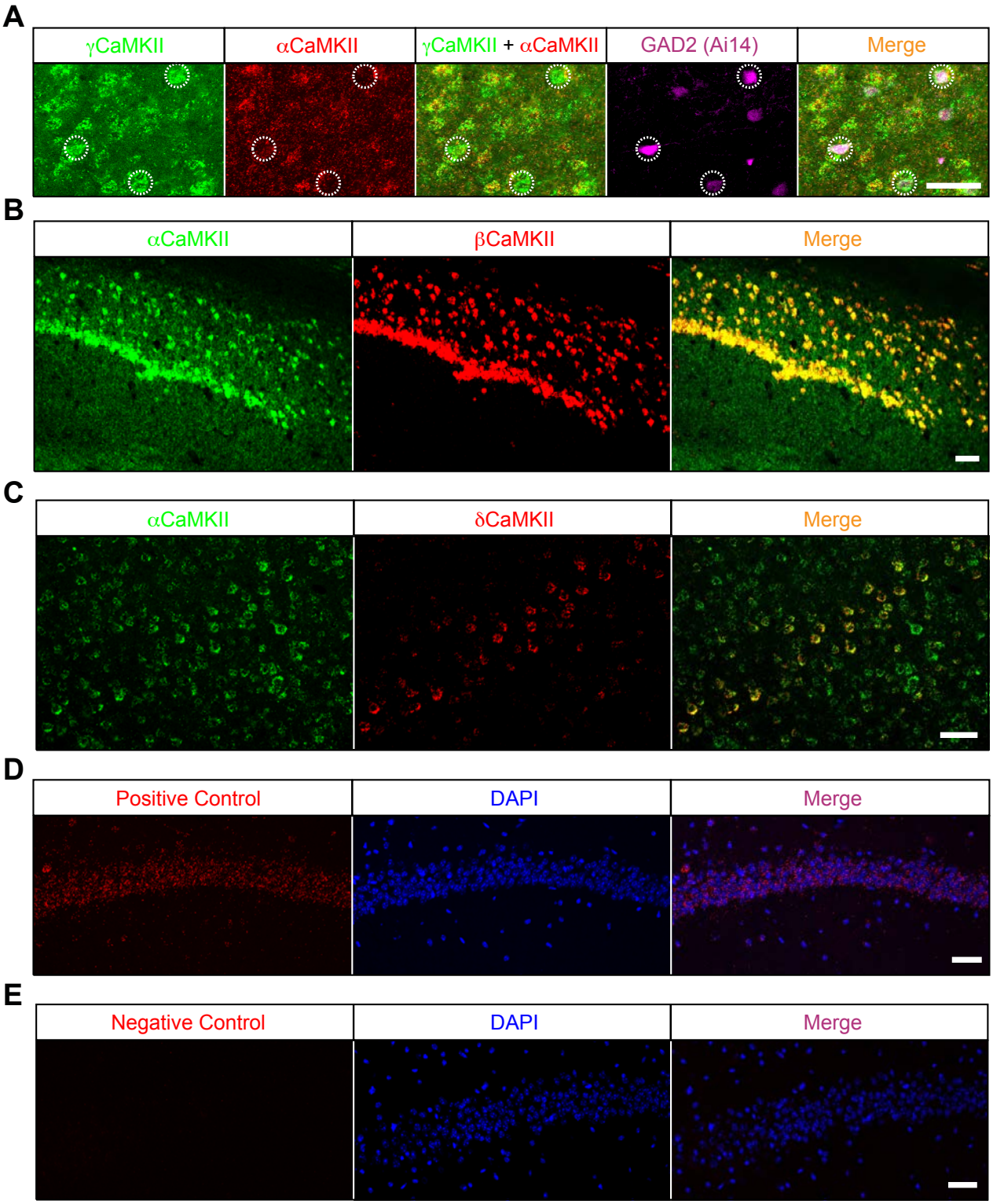

Figure S1 (Related to Figure 2). Expression of various CaMKII isoforms at the mRNA level

(A) γCaMKII mRNA is enriched in αCaMKII-negative/GAD2-positive cortical (the S1 cortex-trunk region) neurons (dashed circles).

(B and C) βCaMKII (in the hippocampus, B) and δCaMKII (in the S1 cortex, C) (red) are expressed specifically in αCaMKII-expressing neurons (green).

(D and E) The housekeeping gene PPIB (D) and the bacterial gene DapB (E) were used as positive and negative controls, respectively; the nuclei were counterstained with DAPI. Scale bar: 50 μm.

Figure S2.

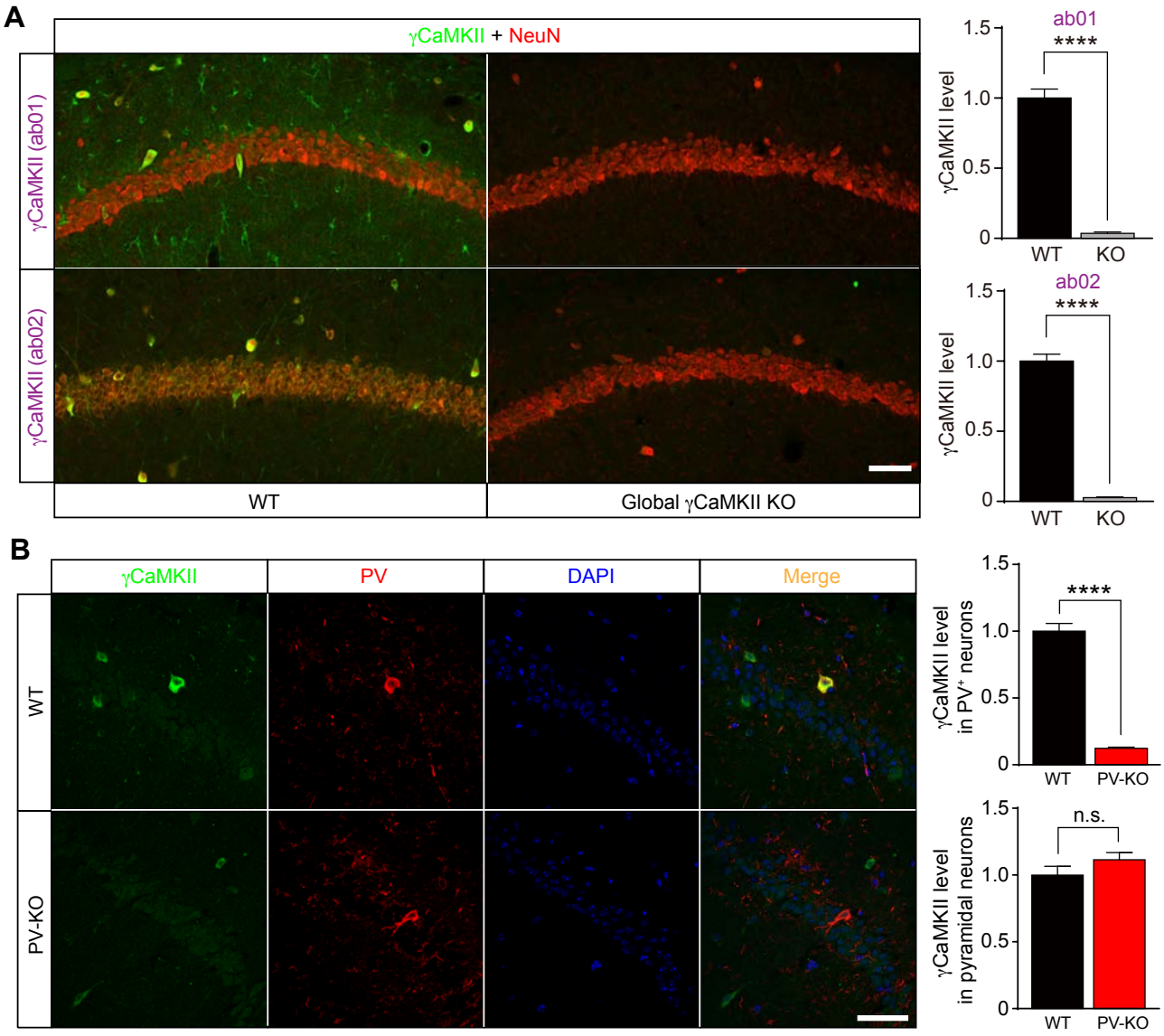

Figure S2 (Related to Figure 2). Specific detection and manipulation of γCaMKII

(A) Hippocampal sections of WT and global γCaMKII-KO mice were stained with NeuN (red) and the ab01 or ab02 antibodies against γCaMKII (green), respectively; summary data are shown at the right (n=27-64 cells from 3 mice/group).

(B) Hippocampal sections of WT and PV-KO mice were immunostained for γCaMKII (green) and PV (red); the nuclei were counterstained with DAPI. The summary data at the right shows γCaMKII immunoreactivity in PV^+ neurons and neighboring pyramidal neurons (n=28-40 cells from 3 mice/group). ****p<0.0001 (unpaired Student's t-test). Scale bar: 50 μm.

Figure S3.

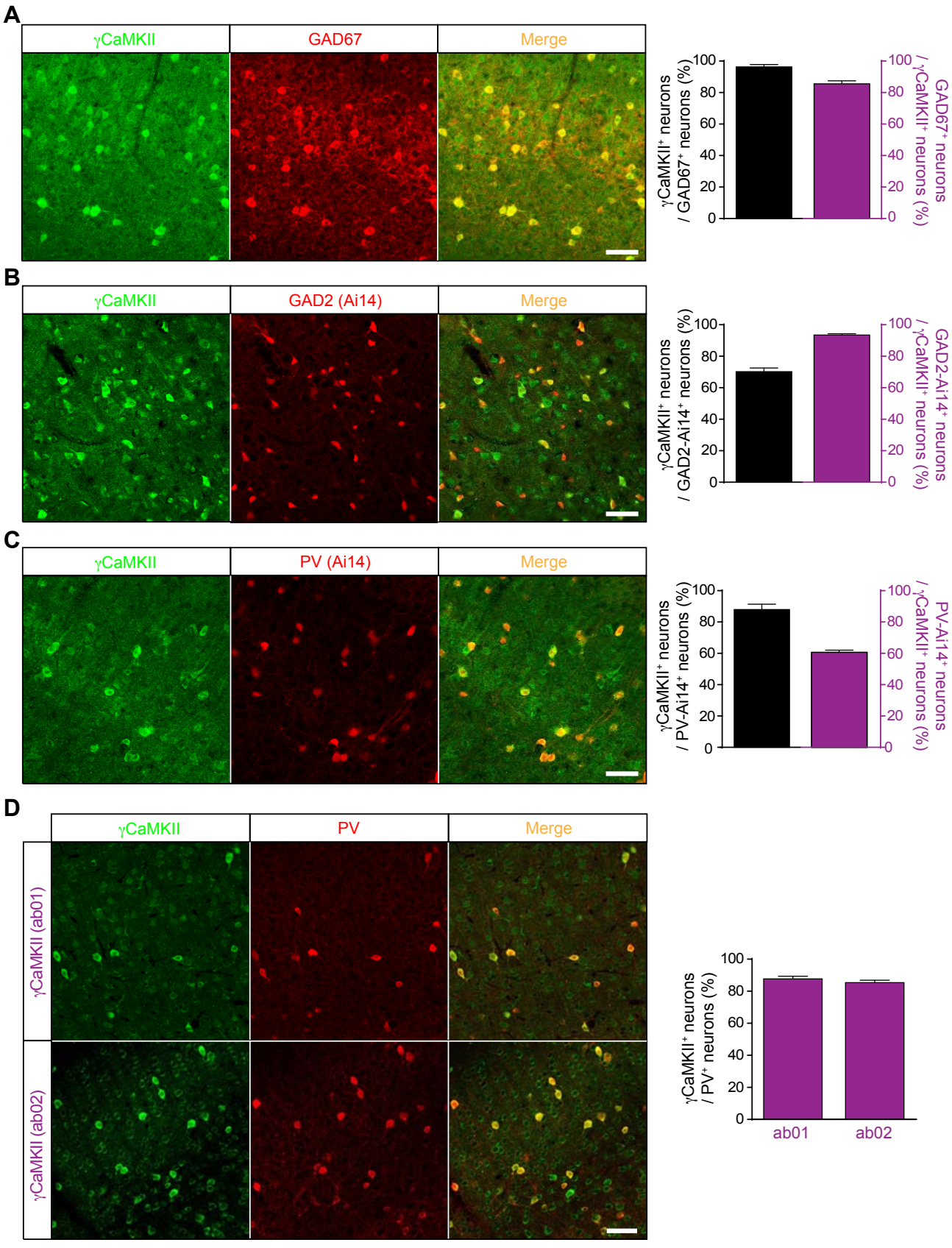
A
γCaMKII
GAD67
Merge
γCaMKII+ neurons / GAD67+ neurons (%)
GAD67+ neurons / γCaMKII+ neurons (%)
B
γCaMKII
GAD2 (Ai14)
Merge
γCaMKII+ neurons / GAD2-Ai14+ neurons (%)
GAD2-Ai14+ neurons / γCaMKII+ neurons (%)
C
γCaMKII
PV (Ai14)
Merge
γCaMKII+ neurons / PV-Ai14+ neurons (%)
PV-Ai14+ neurons / γCaMKII+ neurons (%)
D
γCaMKII
PV
Merge
γCaMKII (ab01)
γCaMKII (ab02)
γCaMKII+ neurons / PV+ neurons (%)
ab01
ab02

Figure S3 (Related to Figure 2). γCaMKII expression in GAD67$^+$, GAD2$^+$, and PV$^+$ interneurons

(A-C) Representative images (left) of neurons co-stained for γCaMKII together with GAD67 (A), GAD2-Ai14 (B), or PV-Ai14 (C) in the cortex and co-expression summary (right) (n=3 sections/group).

(D) Left, representative images showing γCaMKII co-immunostaining with the ab01 or ab02 antibody together with PV$^+$ interneurons in the cortex. Right, summary of co-expression between the γCaMKII antibodies and PV immunostaining (n=3 sections/group). Note that data in both the hippocampus and cortex are included in the summary. Data were analyzed using an unpaired Student's *t*-test. Scale bar: 50 μm.

Figure S4.

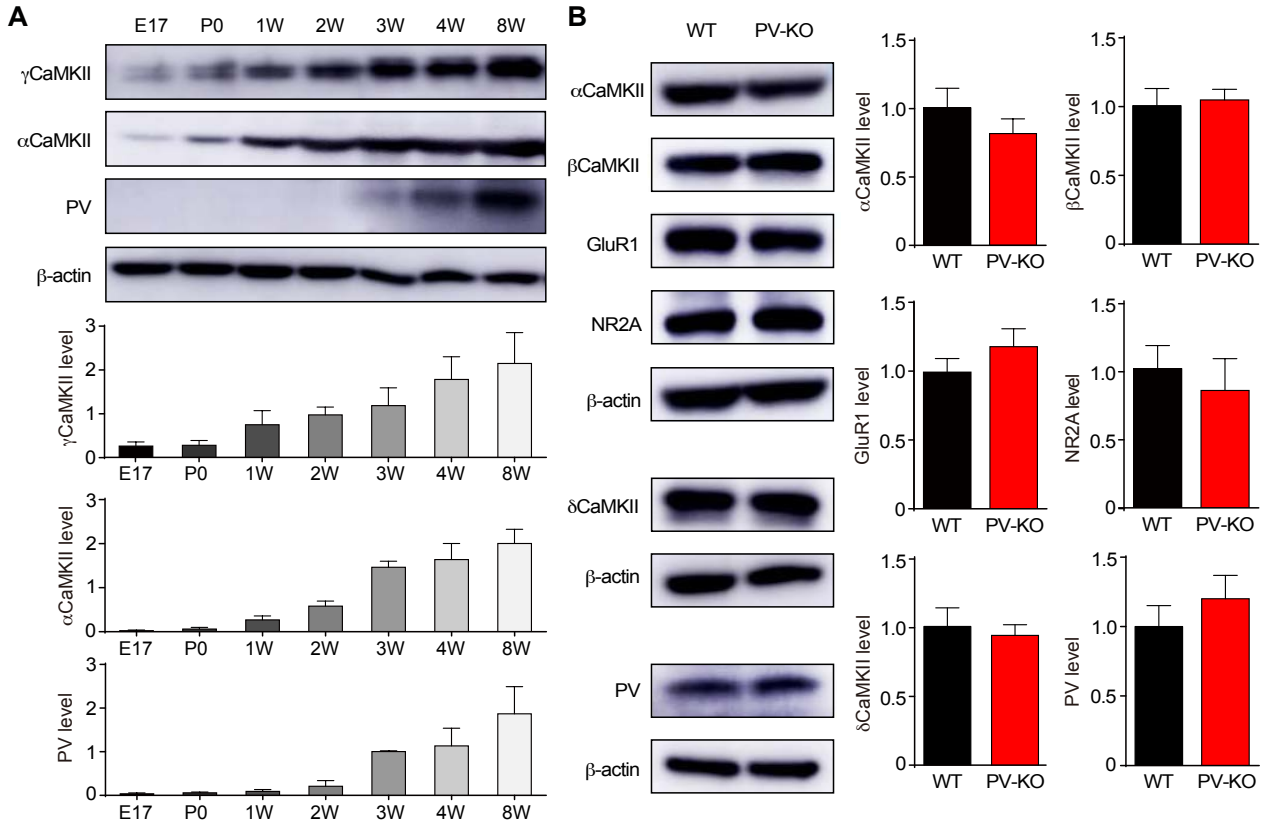

Figure S4 (Related to Figure 3). Expression of γCaMKII and activity-related molecules during development

(A) Western blot analysis of γCaMKII, αCaMKII and PV measured in the hippocampus of mice at the indicated ages (n=3 mice/group).

(B) Western blot analysis of αCaMKII, βCaMKII, δCaMKII, PV, GluR1, and NR2A in the hippocampus of 60-day-old WT and γCaMKII PV-KO mice (n=3-6 mice/group). Data were analyzed using an unpaired Student's *t*-test.

Figure S5.

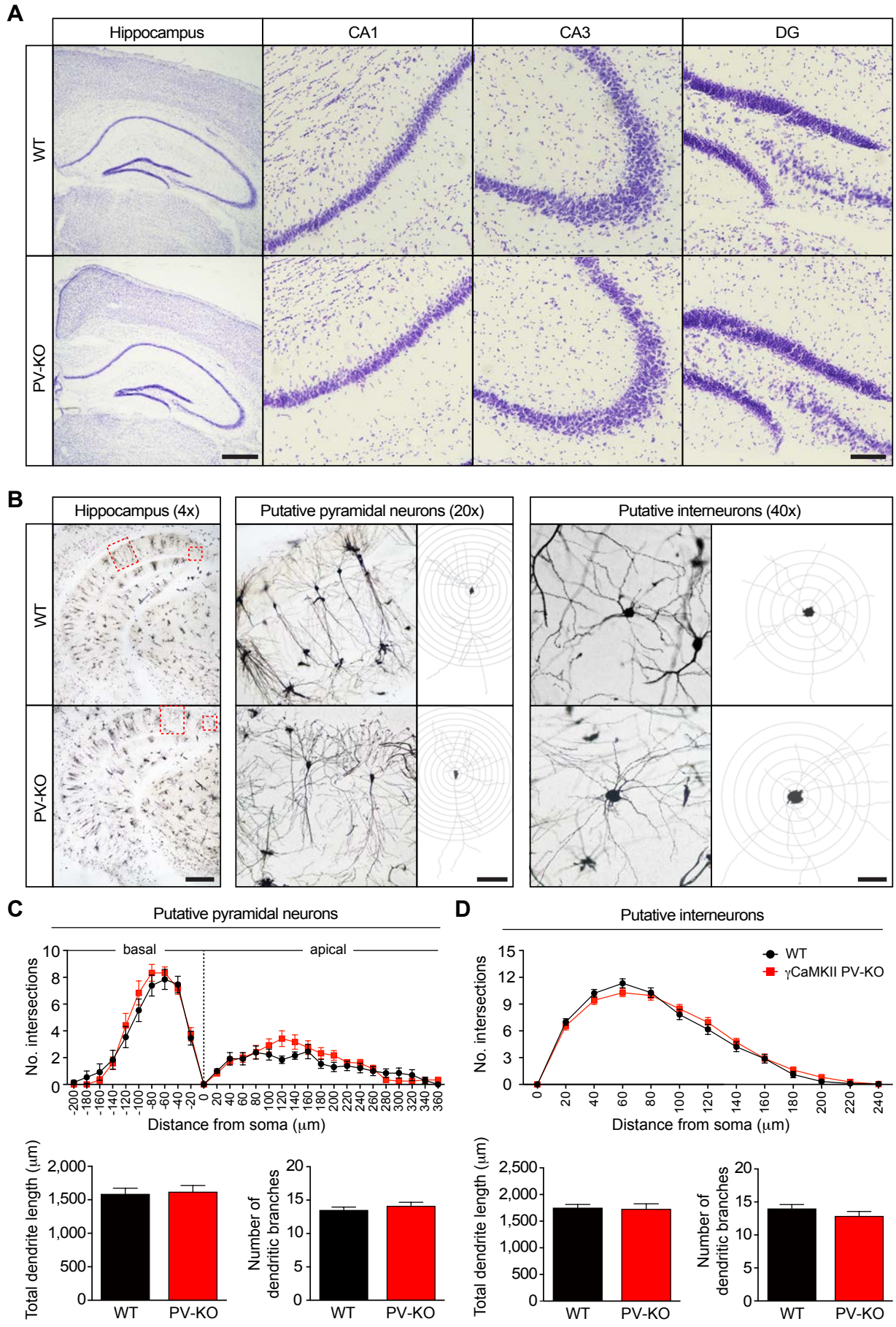
A
Hippocampus
CA1
CA3
DG
WT
PV-KO
B
Hippocampus (4x)
Putative pyramidal neurons (20x)
Putative interneurons (40x)
WT
PV-KO
C
Putative pyramidal neurons
basal
apical
No. intersections
Distance from soma (μm)
Total dendrite length (μm)
Number of dendritic branches
WT
PV-KO
D
Putative interneurons
WT
γCaMKII PV-KO
No. intersections
Distance from soma (μm)
Total dendrite length (μm)
Number of dendritic branches
WT
PV-KO

Figure S5 (Related to Figure 3). γCaMKII PV-KO mice have normal brain morphology and neuronal morphology

(A) Nissl staining of the hippocampus in WT and γCaMKII PV-KO mice; the images at the right show magnified views of the indicated regions.

(B) Representative images of Golgi-stained sections showing the morphology of putative pyramidal neurons and interneurons in the hippocampus of WT and PV-KO mice.

(C and D) Summary of the number of intersections (sholl analysis), total dendrite length and the number of dendrite branches in hippocampal pyramidal neurons (C) and interneurons (D) measured in WT and PV-KO mice (n=13-21 cells/group). Scale bars in A: 500 μm (hippocampus) and 100 μm (CA1, CA3, and DG images); scale bars in B: 500 μm (4x), 100 μm (20x), and 50 μm (40x). Data were analyzed using an unpaired Student's *t*-test.

Figure S6.

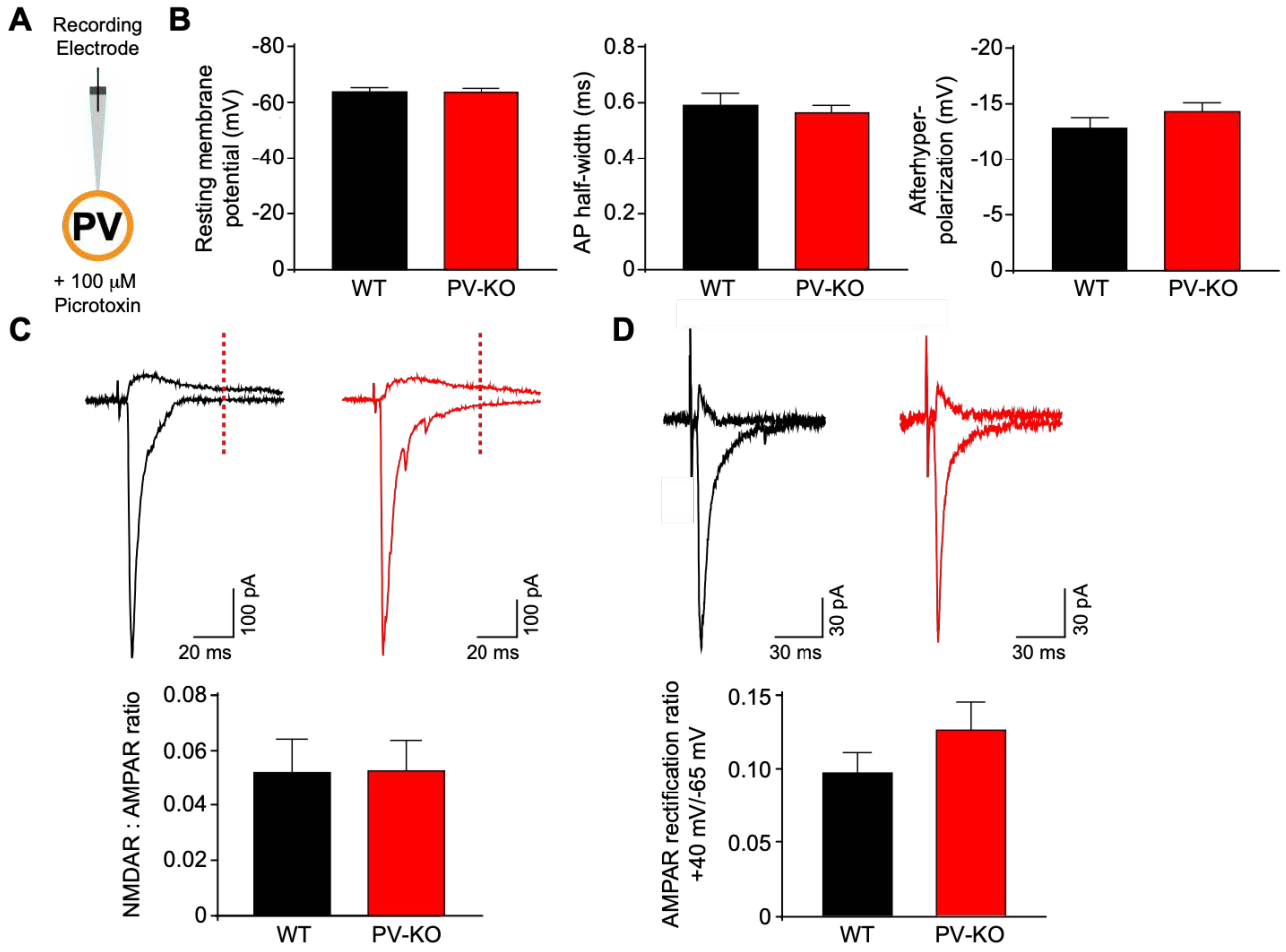

Figure S6 (Related to Figure 3). Hippocampal PV$^+$ interneurons in γCaMKII PV-KO mice have normal baseline synaptic transmission

(A) Schematic illustration of recordings in PV$^+$ interneurons.

(B) Summary of resting membrane potential (left), action potential (AP) half-width (middle), and afterhyperpolarization amplitude (right) in WT and PV-KO neurons (n=5-11 cells from 2-3 mice/group).

(C) Example traces of AMPAR EPSCs recorded at −65 mV and dual component EPSC at +40 mV in WT (black) and PV-KO (red) PV$^+$ interneurons; shown at the bottom is the NMDAR/AMPAR EPSC ratio (n=6-8 cells from 4-6 mice/group). Of note, NMDA currents were relatively low in these neurons (Akgul and McBain, 2016), which, however, should not prevent the local recruitment of CaMKII for generating LTP (Wang and Kelly, 2001)

because CaMKII activation only requires a rise of local calcium near the channels (Ma et al., 2014).

(D) Example traces of AMPAR EPSCs recorded at -65 mV and +40 mV in WT (black) and PV-KO (red) neurons; shown at the bottom is the average AMPAR rectification ratio (n=8-13 cells from 3-4 mice/group). Data were analyzed using an unpaired Student's *t*-test.

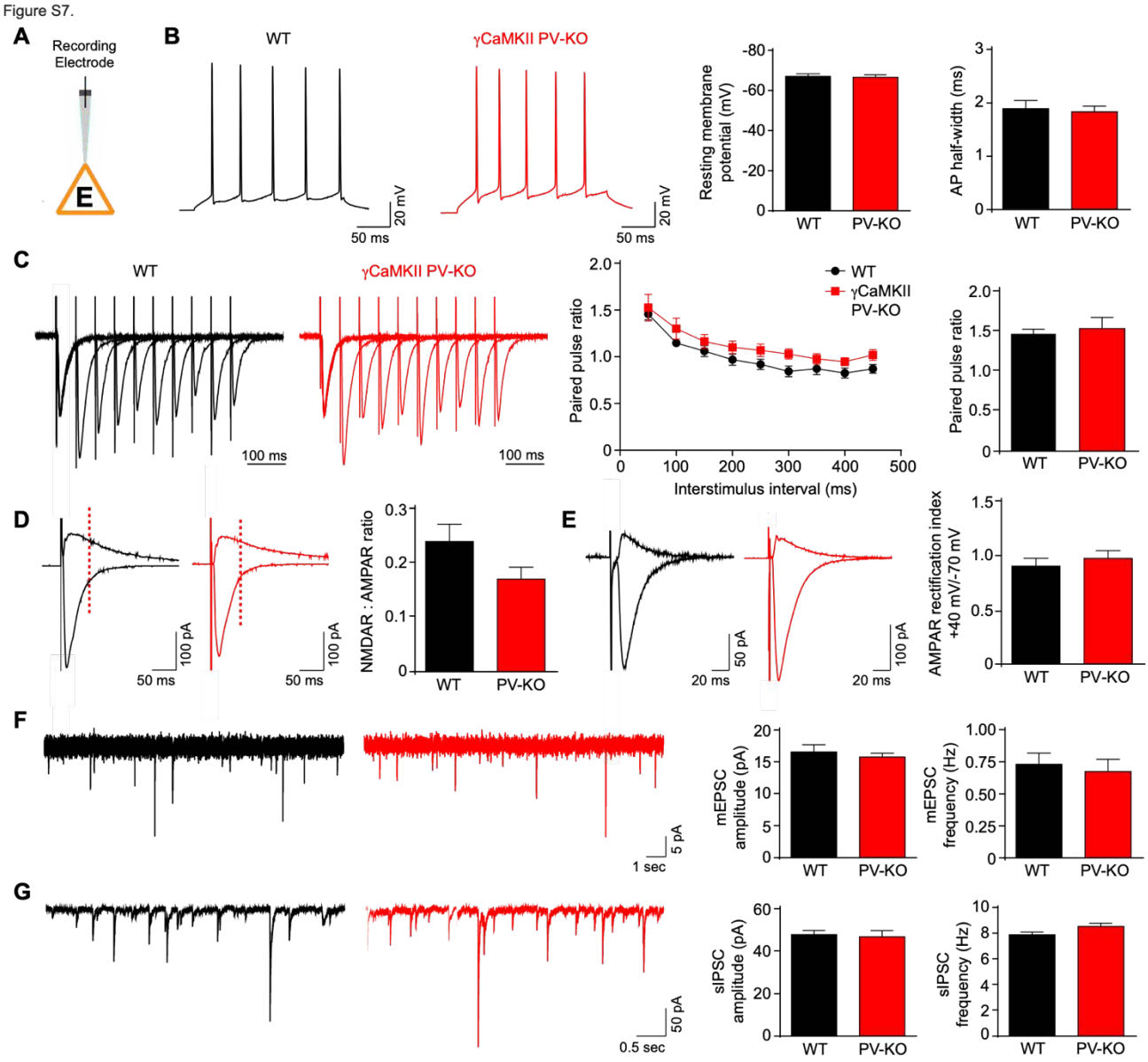

Figure S7 (Related to Figure 3). Pyramidal neurons in γCaMKII PV-KO mice have normal basic membrane properties and synaptic transmission

(A) Schematic illustration of recordings in pyramidal (excitatory) neurons.

(B) Representative traces of evoked action potentials (left) and summary of resting membrane potential and AP half-width (right) in pyramidal cells from WT and PV-KO mice (n=7-8 cells from 2-3 mice/group).

(C) Representative traces (left) and summary of paired-pulse ratio measured at the indicated interstimulus intervals and an interval of 50 ms (right) in pyramidal cells from WT and PV-KO mice (n=7 cells from 2 mice/group).

(D) Example traces of AMPAR EPSCs recorded at -70 mV and dual component EPSC at +40 mV in pyramidal cells from WT (black) and PV-KO (red) mice; shown at the right is the summary of NMDAR/AMPAR EPSC ratio (n=18-25 cells from 6-8 mice/group).

(E) Example traces of AMPAR EPSCs recorded at -70 mV and +40 mV in pyramidal cells from WT (black) and PV-KO (red) mice; shown at the right is the average AMPAR rectification index (n=7 cells from 3-4 mice/group).

(F and G) Example traces of mEPSCs (F) or sIPSC (G) recorded in pyramidal cells from WT (black) and PV-KO (red) mice; shown at the right are the mEPSC (F) or sIPSC (G) amplitude and frequency (n=8-14 cells from 3-4 mice/group). Data were analyzed using an unpaired Student's *t*-test.

Figure S8.

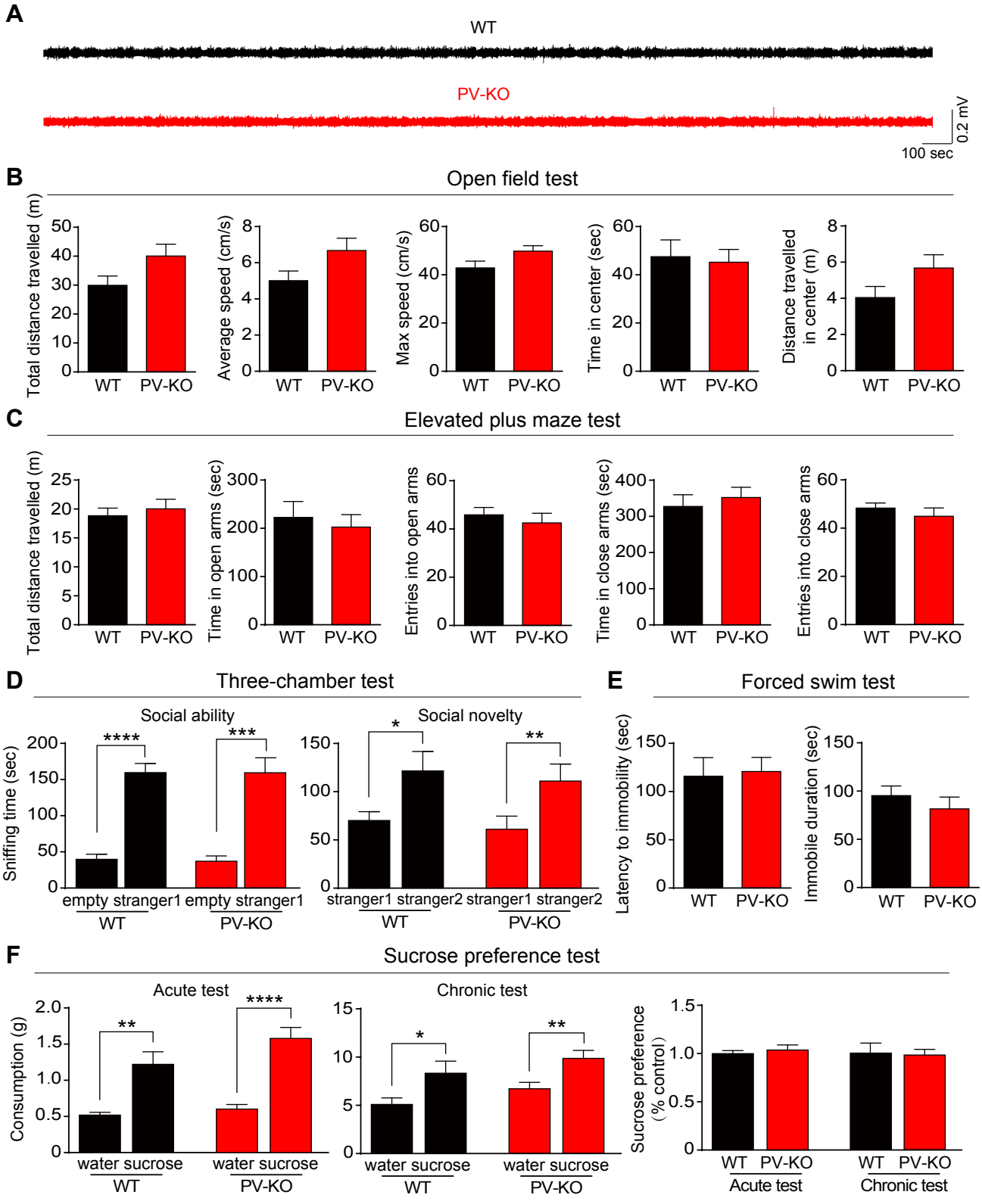
A
WT
PV-KO
0.2 mV
100 sec
B
Open field test
Total distance travelled (m)
Average speed (cm/s)
Max speed (cm/s)
Time in center (sec)
Distance travelled in center (m)
WT
PV-KO
C
Elevated plus maze test
Total distance travelled (m)
Time in open arms (sec)
Entries into open arms
Time in close arms (sec)
Entries into close arms
D
Three-chamber test
Social ability
Social novelty
Sniffing time (sec)
empty stranger1
stranger1 stranger2
E
Forced swim test
Latency to immobility (sec)
Immobile duration (sec)
F
Sucrose preference test
Acute test
Chronic test
Consumption (g)
water sucrose
Sucrose preference (% control)

Figure S8 (Related to Figure 4). γCaMKII PV-KO mice exhibit normal locomotor activity, anxiety, social ability, and depression-like behavior

(A) Representative LFP traces (high-pass filtered at 5 Hz) for analyzing epileptiform events. WT and PV-KO mice didn't show seizure-like behaviors on videotape in a 24 hr session (n=6-8 mice/group).

(B) Summary of total distance travelled, average speed, maximum speed, time spent in the center, and distance travelled in the center for WT and γCaMKII PV-KO mice in the open field test (n=8-9 mice/group).

(C) Summary of the results of the elevated plus maze test in WT and PV-KO mice (n=9-10 mice/group).

(D) Summary of social ability and social novelty measured in WT and PV-KO mice using the three-chamber test (n=8-11 mice/group).

(E and F) Summary of the forced swim test, sucrose preference test in WT and PV-KO mice (n=7-12 mice/group). *p<0.05, **p<0.01, ***p<0.001, and ****p<0.0001 (unpaired or paired Student's t-test).

Figure S9.

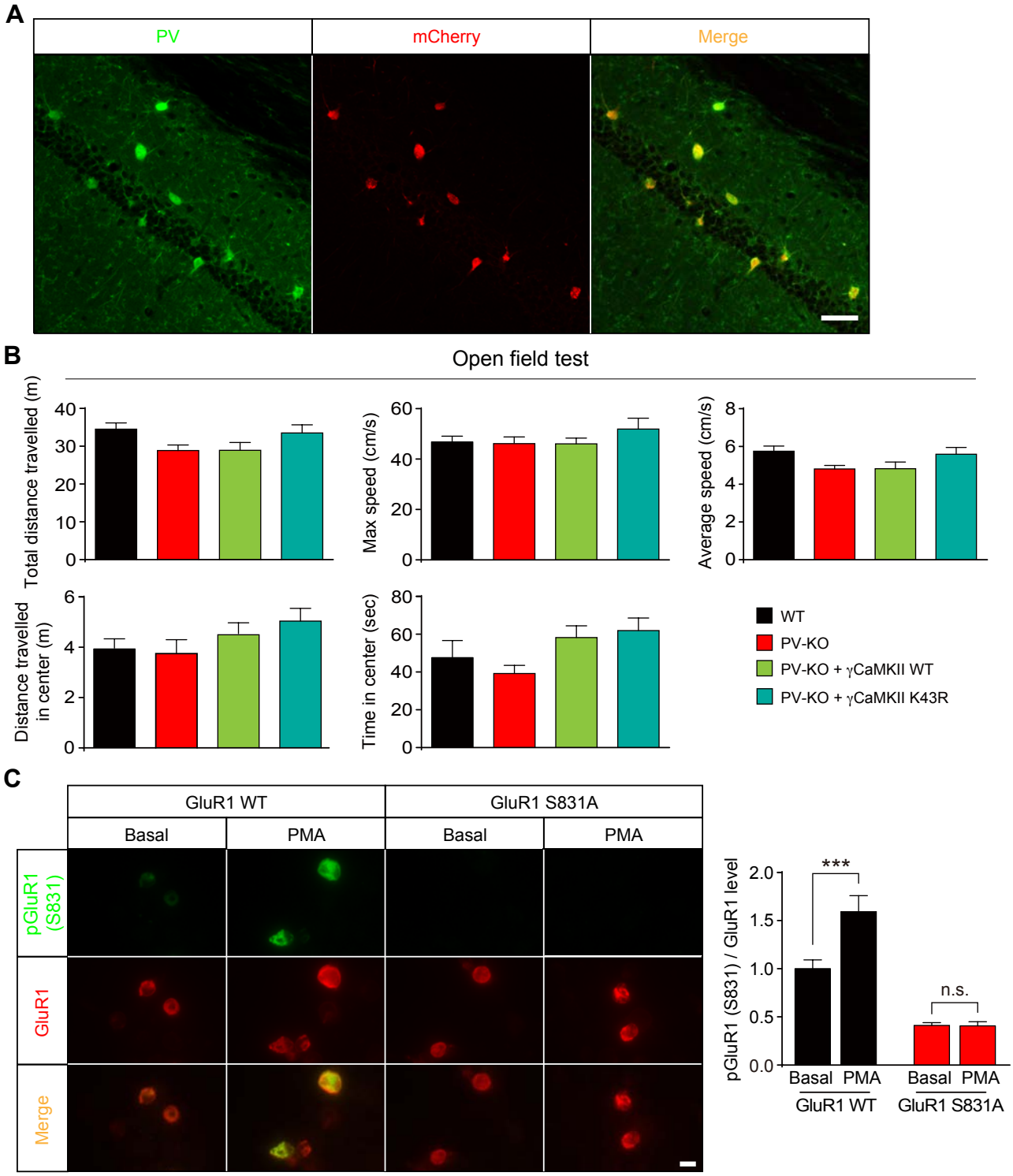
A
PV
mCherry
Merge
B
Open field test
Total distance travelled (m)
Max speed (cm/s)
Average speed (cm/s)
Distance travelled in center (m)
Time in center (sec)
WT
PV-KO
PV-KO + γCaMKII WT
PV-KO + γCaMKII K43R
C
GluR1 WT
GluR1 S831A
Basal
PMA
pGluR1 (S831)
GluR1
Merge
pGluR1 (S831) / GluR1 level
***
n.s.
Basal PMA
GluR1 WT
Basal PMA
GluR1 S831A

Figure S9 (Related to Figures 5 and 6). Virus-mediated overexpression of γCaMKII in hippocampal PV$^+$ interneurons for CFC tests and the specificity of GluR1 phospho-S831 staining

(A) Representative images showing that target genes delivered with the virus (red) are specifically expressed in hippocampal PV$^+$ interneurons (green). Scale bar: 50 μm.

(B) The open field test was conducted after CFC test in order to examine the locomotor activity and anxiety levels in WT mice, γCaMKII PV-KO mice, and PV-KO mice injected with a virus expressing WT or K43R γCaMKII (n=8 mice/group). The virus-mediated overexpression did not affect the locomotor activity and anxiety levels after CFC test.

(C) Representative images (left) and summary data (right) of phosphorylated GluR1 (S831) measured in HEK293 cells expressing GluR1 WT or GluR1 S831A under basal conditions or after PMA stimuli. As shown previously (Diering et al., 2016), PMA significantly increased the staining intensity of antiphospho-S831 in GluR1 WT cells but not S831A cells (n=30 cells/group). Scale bar: 10 μm. ***p<0.0001 (one-way ANOVA followed by Tukey's test).

Figure S10.

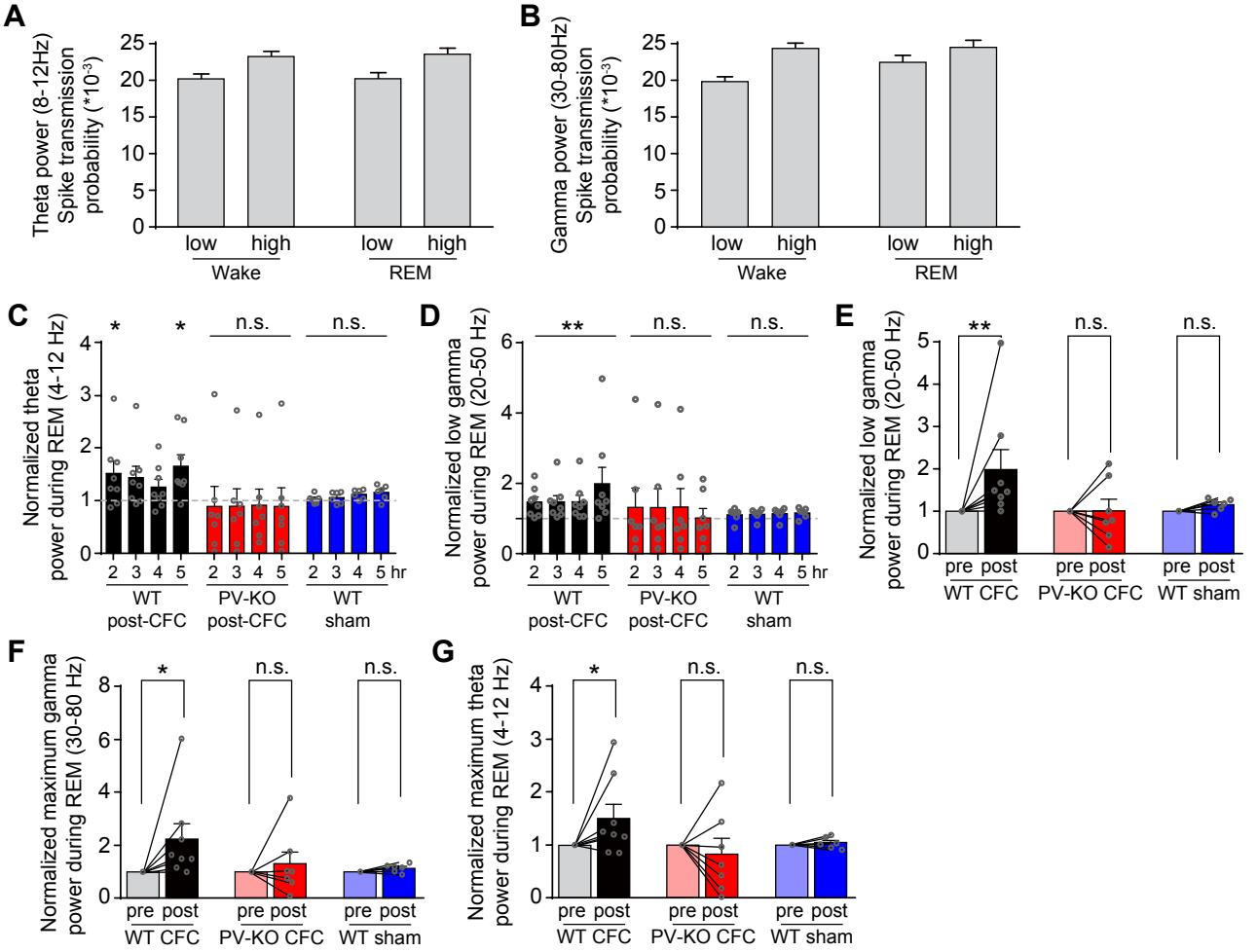

Figure S10 (Related to Figure 7). LFP power changes during REM sleep following CFC.

(A and B) CCGs were calculated during low and high theta states (median split) and during low and high gamma states, during wake and REM sleep. Spike transmission probability was enhanced when LFP power was high, for both theta (N=2284, Mann–Whitney U test, all $p<6.7^{-4}$) and gamma (N=2284, Mann–Whitney U test, all $p<2.1^{-15}$) filtered LFP, and during both waking and REM (n=6 mice/group).

(C-E) Summary of theta (4-12 Hz) and low gamma (20-50 Hz) in REM before and after CFC. (C and D) Data in REM were analyzed over a period of 2 hr, 3 hr, 4 hr and 5 hr before and after CFC training in WT, PV-KO, and sham-treated WT mice.

(F and G) Summary of maximum gamma (30-80 Hz) and maximum theta (4-12 Hz) during REM before and after CFC in WT, PV-KO, and sham-treated WT mice (n=6-8 mice/group). *p<0.05 and **p<0.01 (Wilcoxon matched-pairs signed rank test).

Figure S11.

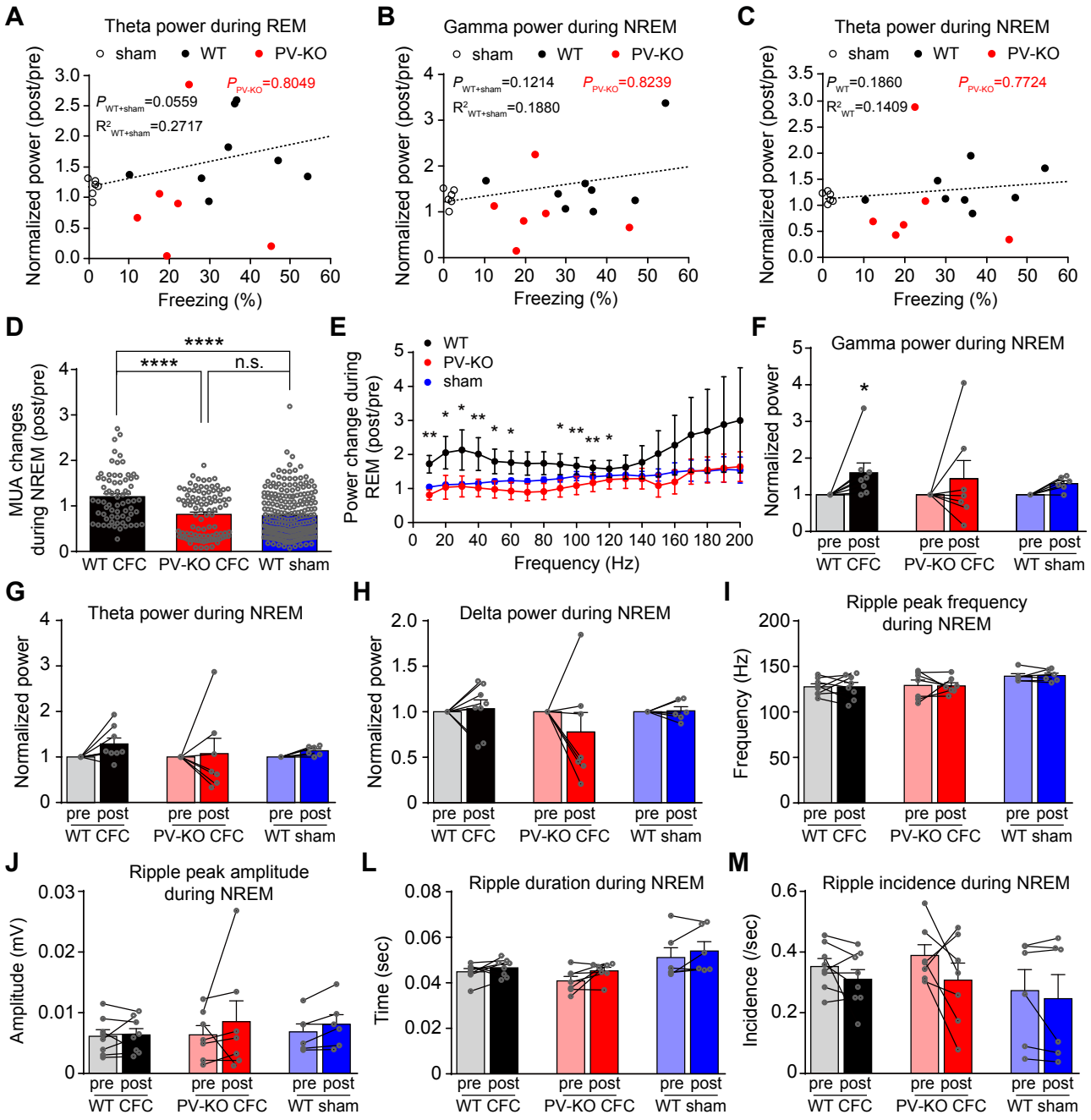

Figure S11 (Related to Figure 7). Oscillation changes and their correlation with memory performance

(A) Changes of theta band power (post/pre) during REM are plotted against freezing (%) for each WT, PV-KO, and sham-treated WT mouse. Black circles: the WT sham group (n=6 mice), black dots: the WT group (n=8 mice), red dots: PV-KO group (n=6 mice).

(B) Changes of gamma band power (post/pre) during NREM are plotted against freezing (%) for each WT, PV-KO, and sham-treated WT mouse.

(C) Changes of theta band power (post/pre) during NREM are plotted against freezing (%) for each WT, PV-KO, and sham-treated WT mouse.

(D) Summary of MUA changes (post/pre) for FSIs during NREM (the first 60 sec for each NREM); compared to the groups of PV-KO and sham-treated WT mice, MUAs of FSIs increased significantly in the WT group following CFC (n=69-228 NREMs from 2-4 mice/group). ****$p<0.0001$, one-way ANOVA test followed by Tukey's test.

(E) Average power changes (post/pre) during REM were measured in WT, PV-KO, and sham-treated WT mice at frequencies ranging from 0 to 200 Hz, the bin size is 10 Hz (n=6-8 mice/group). *$p<0.05$ and **$p<0.01$, Wilcoxon matched-pairs signed rank test.

(F-H) Normalized gamma wave (30-80 Hz) (F), theta wave (4-12 Hz) (G) and delta wave (1-4 Hz) (H) power during NREM before and after CFC training in WT, PV-KO, and sham-treated WT mice (n=6-8 mice/group). *$p<0.05$, Wilcoxon matched-pairs signed rank test.

(I-M) Summary of ripple (100-200 Hz) peak frequency (I), peak amplitude (J), duration (L) and incidence (M) before and after CFC (n=6-8 mice/group). Data were analyzed using Wilcoxon matched-pairs signed rank test. For A-C, the Bonferroni-corrected *p*-values indicate the results of a Spearman rank order test.

sFigure 12.

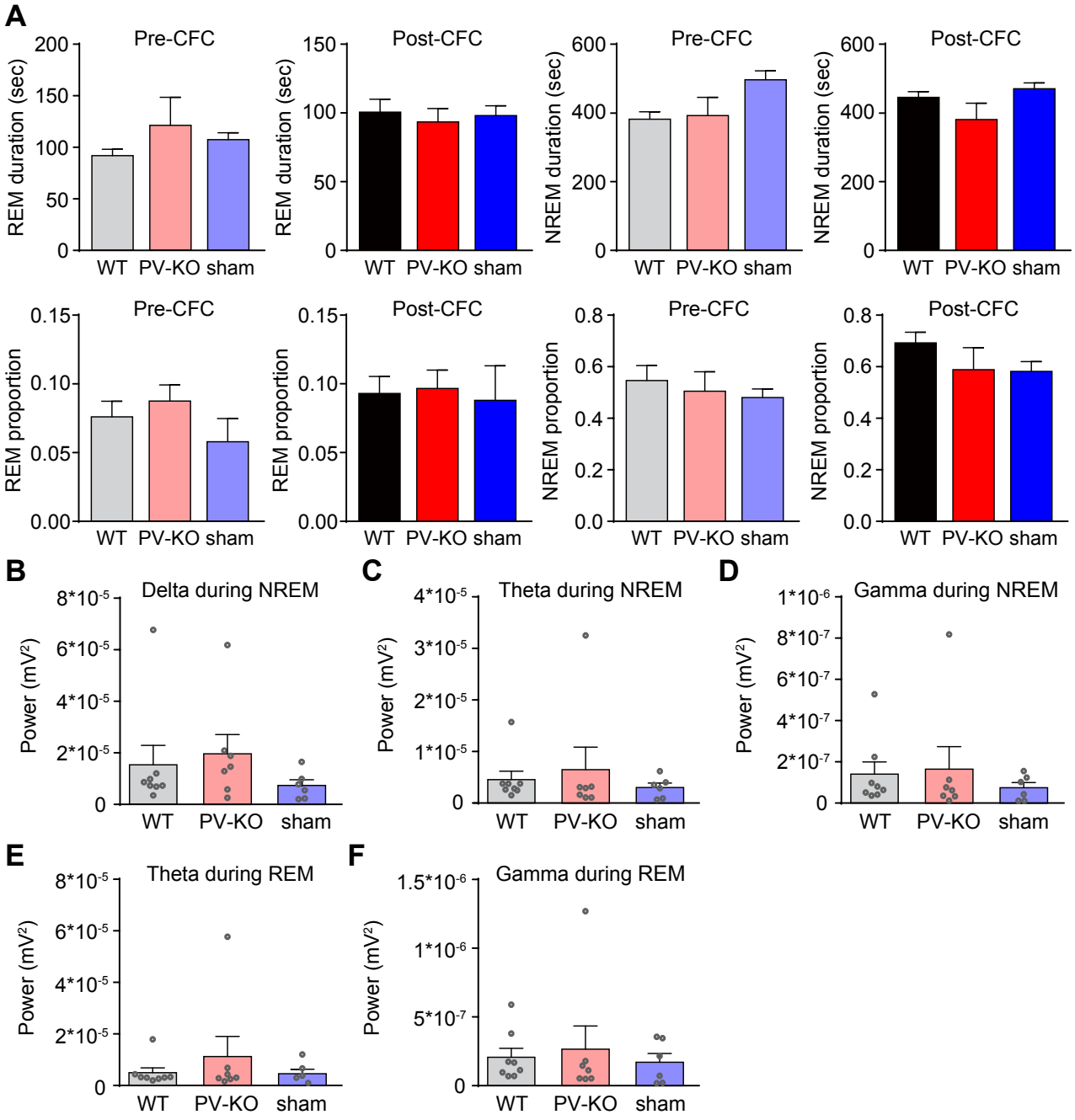

Figure S12 (Related to Figure 7). Sleep conditions and pre-training network oscillations in γCaMKII PV-KO mice

(A) Summary of the episodic duration and the proportion for REM (left) and NREM (right) sleep before and after CFC (n=6-8 mice/group).

(B-D) Summary of power values for pre-CFC delta (1-4 Hz) (B), theta (4-12 Hz) (C) and gamma (30-80 Hz) (D) waves measured during NREM sleep in WT, γCaMKII PV-KO, and sham-treated WT mice.

(E and F) Summary of power values for pre-CFC theta (E) and gamma (F) waves measured during REM sleep. Data were analyzed using a one-way ANOVA followed by Tukey’s test.